The Journal of Chemical Physics

RESEARCH ARTICLE | APRIL 22 2025

Dynamic phases of synthetic bath at negative temperatures

Guo-hao Xu ; Jiarui Zeng; Yao Yao

J. Chem. Phys. 162, 164303 (2025)
https://doi.org/10.1063/5.0259817

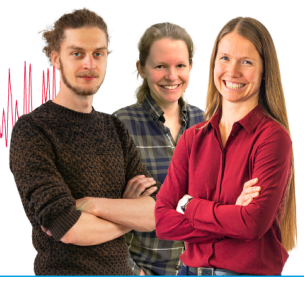

AIP Publishing

The Journal of Chemical Physics ARTICLE pubs.aip.org/aip/jcp

Dynamic phases of synthetic bath at negative temperatures

Cite as: J. Chem. Phys. 162, 164303 (2025); doi: 10.1063/5.0259817
Submitted: 21 January 2025 • Accepted: 7 April 2025 •
Published Online: 22 April 2025

Guo-hao Xu,[1] Jiarui Zeng,[2] and Yao Yao[3,a)]

AFFILIATIONS

[1] Department of Physics, South China University of Technology, Guangzhou 510640, China
[2] School of Physics and Optoelectronic Engineering, Hainan University, Haikou 570228, China
[3] Department of Physics, South China University of Technology, Guangzhou 510640, China and State Key Laboratory of Luminescent Materials and Devices, South China University of Technology, Guangzhou 510640, China

[a)] **Author to whom correspondence should be addressed:** yaoyao2016@scut.edu.cn

ABSTRACT

Quantum thermal devices are typically designed to perform work beyond classical ability, with their potential to utilize quantum coherence as a resource. Here, we investigate that an energy-carrying molecular model for donor and acceptor coupling to two physical baths and an external driving field offers diverse functions transformed among heat engine, refrigerator, and thermal accelerator. The counter-rotating component of the driving field can induce behavior where the heat flows from the cold bath to the hot one and an output work is done. It is, thus, evident that the precise modulation of the synthetic bath whose inverse temperature varies continuously from negative to positive enables all modes of energy transfer in the phase diagram. The non-equilibrium quantum thermodynamics for realistic devices is further investigated when the external driving field is switched on and off periodically.

I. INTRODUCTION

Quantum thermodynamics has attracted great attention during the past several decades.[1,2] Quantum thermal devices, utilizing quantum systems under periodic external drive as working substances and embedded in two baths at different temperatures, follow the principles of quantum thermodynamics to manipulate thermal energy in ways that might be forbidden for classical devices, potentially achieving higher power conversion efficiencies. They have hitherto been realized in a number of quantum simulators, such as trapped ions,[3–5] nitrogen vacancy centers,[6–8] ultracold atoms,[9–11] superconducting circuits,[12–16] and so on (Refs. 17–27), to investigate their unique properties. However, experiments often focus on individual tasks that quantum thermal devices can perform without fully considering their ability to change and adapt functions. Systematic research to clarify the relevance of various functions is still lacking, and a fully functional map to handle the energy flow could be confidently helpful.

The synthetic bath temperature and the external driving field are critical factors leading to rich phases in quantum thermal devices. The quantum heat engine, as a common prototype of quantum thermal devices, can be regarded as associated with a bath at negative temperatures,[28] in which population-inverted systems exhibit larger populations on higher energy levels.[29] Negative temperature is not only compatible with equilibrium thermodynamics but also with non-equilibrium thermodynamics.[30] Despite the extensive and profound investigations of population-inverted systems in the literature, there remains a fundamental question: how to build up such a nontrivial bath with arbitrary negative temperatures, which long-termly serves as a subject of controversy.[31] Struchtrup realized a population-inverted state is able to act as a work repository but has thermal instability.[32] On the other hand, a bath at a negative temperature in the absence of an external drive was successfully achieved by Bera *et al.* through constructions with two baths at positive temperatures.[33] That is, the populations of two states in the quantum system can reach an equilibrium corresponding to negative synthetic temperature.

In addition, the influence of the external driving field was also comprehensively discussed. When the external drive is acting on negative-temperature systems, the baths at negative temperatures can do the work, and the external drive will be enhanced by the population inversion rather than conventionally reduced.[34] In the

negative-temperature regime, population inversion is present, and the system can store and, subsequently, deliver work in a manner that is fundamentally different from classical systems. Subsequently, masers have, thus, become a prototype and foundation for studying continuous quantum heat engines.[35–41] A three-level model can appropriately describe realistic masers,[42–45] and the rotating wave approximation is widely considered in Refs. 46 and 47. Recently, an approach has been proposed that employs two-photon Raman transitions in a three-level system to create a negative temperature bath, demonstrating that coherent heat transfer with baths yields significant quantum enhancements in performance.[48] When optimized via an external drive by exploiting quantum coherence, the quantum thermal devices might deliver efficiencies that challenge conventional thermodynamic limits while also regulating entropy production and minimizing irreversible losses.

Generally speaking, the direction of heat and work flows could be used to classify quantum thermal devices, and the thermalization of baths has a significant impact on the energy transformation.[49] Achieving multifunctionality in quantum thermal devices, therefore, requires a comprehensive study of how the temperature of the bath and the driving field affect the direction of energy flow. Molecules in solutions or cavities hold extremely long quantum coherence[50–54] so that they can perform as a perfect work substance to reveal photoinduced energy carrying mechanisms between donor and acceptor units interacting with thermal light and, thus, act like a maser.[55] The impact of an external driving field on molecular systems with negative synthetic temperatures warrants further discussion. In this paper, therefore, we model a donor–acceptor molecule as a three-level system to explore the multiple functionalities of a single quantum thermal device from the perspective of a dynamic phase diagram. Two physical baths, both at positive temperatures, coupled to the molecule to synthesize a bath at negative inverse temperature. When the external drive is introduced to the synthetic bath, energy transfers will be found to differ completely from that of the classical counterpart. While Ref. 33 provides a comprehensive study of steady-state thermodynamics in a three-level system with synthetic negative temperatures, our work extends these results by incorporating an external driving field that induces shifts among distinct operational modes, such as heat engine, refrigerator, and thermal accelerator. Moreover, our investigation of transient response in quantum thermal devices, particularly under periodic switching of the driving field, offers new insights into energy transfer and work extraction mechanisms beyond the static picture.

The rest of this paper is organized as follows: Sec. II introduces the donor–acceptor molecular model and then defines its heat fluxes and power with the full parameterized Hamiltonian. In Sec. III, we discuss how the synthetic inverse temperature of the baths and external field, respectively, influence the dynamic phases of the system for multiple operations. We also investigate an interesting combined case, with the driving field periodically switched on and off. Finally, Sec. IV draws a conclusion.

II. MODEL AND METHODOLOGY

We model a donor–acceptor molecule as a qutrit system sandwiched in L and R thermal baths, both at positive physical temperatures, as sketched in Fig. 1(a). The donor corresponds to levels $|0\rangle$ and $|2\rangle$, and the acceptor is associated with $|0\rangle$ and $|1\rangle$, with both sharing the common ground state $|0\rangle$. The Hamiltonian of the three-level system is given by

$$H_0 = E_1\sigma_{11} + E_2\sigma_{22}, \tag{1}$$

where $E_{1,2}$ represents the excited energy of $|1,2\rangle$. The intramolecular energy transition operator between two units is defined as $\sigma_{ij} = |i\rangle\langle j|$ where $i,j = 0,1,2$. In the rotating-wave approximation, an external field introduces a time-dependent interaction between the levels $|1\rangle$ and $|2\rangle$, described by the interaction Hamiltonian,[46]

$$V(t) = \lambda(\sigma_{12}e^{i\omega t} + \sigma_{21}e^{-i\omega t}). \tag{2}$$

Herein, λ is the atom-field coupling strength, and ω denotes the frequency of the driving field. Throughout this work, we set the Planck constant $\hbar = 1$ and the Boltzmann constant $k_B = 1$.

The left bath at inverse temperature β_L weakly interacts with the levels $|0\rangle$ and $|2\rangle$, while the right bath at inverse temperature β_R couples to the levels $|0\rangle$ and $|1\rangle$. In the absence of the external field, the populations of the levels at a steady state satisfy $p_0/p_2 = e^{\beta_L E_2}$ and $p_0/p_1 = e^{\beta_R E_1}$. This can be imaged as the levels $|1\rangle$ and $|2\rangle$ interacting with a synthetic bath at inverse temperature $\beta_S = \frac{1}{E_2-E_1}\ln(\frac{p_1}{p_2}) = \frac{\beta_L E_2 - \beta_R E_1}{E_2-E_1}$, and the bath can reach the same temperature after sufficient evolution for thermalization without external driving. We

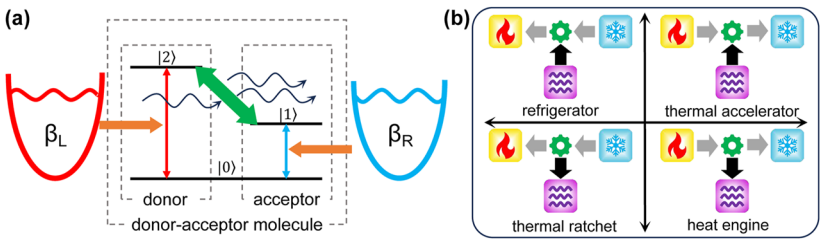

FIG. 1. (a) Schematic of a donor–acceptor molecular thermal device modeled as a three-level system with the donor and acceptor sharing the common ground state $|0\rangle$. The donor corresponding to levels $|0\rangle$ and $|2\rangle$ contacts the left bath at positive inverse temperature β_L, while the acceptor corresponding to levels $|0\rangle$ and $|1\rangle$ couples to the right bath at positive inverse temperature β_R. An external field is introduced between levels $|1\rangle$ and $|2\rangle$ to facilitate the transfer of work. (b) Schematic of four dynamic phases of a quantum thermal device functioning as a refrigerator, thermal accelerator, thermal ratchet, and heat engine. The arrows characterize the directions of heat flows (horizontal) and work flows (vertical), respectively.

assume the baths undergo Markovian time evolution and do not consider thermal energy relaxation, so the qutrit could be appropriate to simulate the energy-carrying molecule. The overall dynamics is then governed by the Lindblad master equation,[56]

$$\dot{\rho} = -i[H(t), \rho] + \mathcal{L}_L(\rho) + \mathcal{L}_R(\rho), \tag{3}$$

where ρ represents the density matrix characterizing the state of the three-level system and the time-dependent Hamiltonian is given by $H(t) = H_0 + V(t)$. The first term on the right-hand side of Eq. (3) refers to the unitary evolution arising from the three-level system Hamiltonian H_0 and the interaction $V(t)$. The second and third terms stand for the dissipative contributions from the left and right baths, respectively, on the system dynamics. The Lindblad superoperators $\mathcal{L}_{L(R)}[\rho]$ are expressed as follows:

$$\begin{aligned}\mathcal{L}_L[\rho] = \Gamma_L(N_L + 1)(\sigma_{02}\rho\sigma_{02}^{\dagger} - 1/2\{\sigma_{02}^{\dagger}\sigma_{02}, \rho\}) \\ + \Gamma_L N_L(\sigma_{02}^{\dagger}\rho\sigma_{02} - 1/2\{\sigma_{02}\sigma_{02}^{\dagger}, \rho\}),\end{aligned} \tag{4}$$

and a similar expression is for $\mathcal{L}_R[\rho]$. Herein, $N_L = 1/(e^{\beta_L E_2} - 1)$ and $N_R = 1/(e^{\beta_R E_1} - 1)$ represent the thermal occupation numbers. The anti-commutator satisfies $\{X, Y\} = XY + YX$, and $\Gamma_{L(R)}$ denotes the Weiskopf–Wigner decay constant.

In terms of the direction of energy transfer, including both heat and work flows, thermal devices can be classified into heat engines, refrigerators, and thermal accelerators.[57] Taking into account the concept of thermal ratchet,[58,59] we can identify four dynamic phases, each corresponding to different operations in a single quantum thermal device, as shown in Fig. 1(b). The heat flows from the hot bath to the cold bath in both heat engines and refrigerators while reversing in the thermal accelerators and thermal ratchets. On the other hand, the work is output from the heat engines and thermal ratchets, whereas it is input to the refrigerators and thermal accelerators.

Theoretically, the energy in quantum thermal devices can be divided into heat and work by examining the time dependencies of the density and Hamiltonian operators.[60–64] Energy fluxes are then distinguished into heat fluxes and power, with power defined by the Hamiltonian superoperator and heat fluxes defined by the dissipative Lindblad superoperator.[46] That is, based on heat exchange between the two baths and the qutrit, the heat flux is defined as

$$\dot{Q} = \mathrm{Tr}\left[\frac{\partial \rho}{\partial t} H(t)\right]. \tag{5}$$

This change in the internal energy due to the evolution of its state reflects the heat variation of the qutrit induced by dissipative processes. Heat flux $\dot{Q} > 0$ implies that heat is delivered into the qutrit system from the synthetic bath, while $\dot{Q} < 0$ means that heat is removed from the qutrit caused by the synthetic bath. In order to distinguish the contributions from the interaction of the qutrit with the left bath and the right bath, the heat flux $\dot{Q}$ can be further separated into two components given by[65]

$$\dot{Q}_{L(R)} = \mathrm{Tr}\left[\mathcal{L}_{L(R)}(\rho) H(t)\right]. \tag{6}$$

The heat is absorbed from the left (right) bath into the qutrit system for $\dot{Q}_{L(R)} > 0$, whereas heat is released from the qutrit system into the left (right) bath for $\dot{Q}_{L(R)} < 0$. Due to the coupling between the qutrit and the driving field, the power is quantified as

$$P = \mathrm{Tr}\left[\rho \frac{\partial H(t)}{\partial t}\right]. \tag{7}$$

The explicit time dependence of the Hamiltonian reveals how the energy of the qutrit is altered by the external field. Negative P represents that work is transferred to the driving field [as illustrated by the directions of the black arrows in the two lower panels of Fig. 1(b)], while positive P indicates that work is supplied to the qutrit by the driving field [as illustrated by the directions of the black arrows in the two upper panels of Fig. 1(b)].

The von Neumann entropy of the qutrit system reads as $S = -\mathrm{Tr}[\rho \log \rho]$, and the change rate of it is defined as entropy flux,

$$\dot{S} = -\mathrm{Tr}\left[\frac{\partial \rho}{\partial t} \log \rho\right]. \tag{8}$$

$\dot{S} > 0$ means that entropy enters the qutrit system from the synthetic bath, while $\dot{S} < 0$ implies that entropy exits from the qutrit into the synthetic bath. The entropy fluxes associated with the left and right baths, respectively, become

$$\dot{S}_{L(R)} = \beta_{L(R)} \dot{Q}_{L(R)}. \tag{9}$$

The change in entropy arises from the heat transferred at a given temperature. Entropy flows from the left (right) bath into the qutrit system for $\dot{S}_{L(R)} > 0$, and from the qutrit system into the left (right) bath for $\dot{S}_{L(R)} < 0$. Then, the overall entropy production rate can be defined as

$$\Sigma = \dot{S} - \dot{S}_L - \dot{S}_R. \tag{10}$$

At a steady state, $\dot{S} = 0$, and the entropy production rate $\Sigma \geq 0$ represents that the second law of thermodynamics is satisfied.

III. RESULTS AND DISCUSSIONS

The diverse phases in quantum thermal devices can be understood as a consequence of the interplay between two key factors: the synthetic bath temperature and the external driving field. We begin with the influence of the synthetic bath temperature on the device operation, revealing transitions among heat engine, refrigerator, and thermal accelerator regimes. The system's entropy under these conditions is also examined. The analysis further addresses the role of the counter-rotating component of the driving field in inducing thermal ratchet behavior. In addition, an experimentally feasible protocol that periodically switches the external driving field on and off is employed to explore the transient energy flow responses of the real thermal device.

All our simulations are under the dimensionless parameter sets $E_1 = 38$, $E_2 = 47.5$, $\Gamma_L = 1$, and $\Gamma_R = 1$, and the energy spacing between levels $|1\rangle$ and $|2\rangle$ takes a constant value of 9.5. Taking a realistic molecule into consideration, this energy spacing can be related to an X-band microwave with 9.5 GHz that is normally utilized in electron paramagnetic resonance, and then other parameters can be relevantly quantified. Techniques such as transient photoluminescence spectroscopy and electron paramagnetic resonance spectroscopy have advanced to a point where one can probe

and even manipulate the energy transfer processes at the molecular scale.[51,54] The pulse-based techniques are well established in quantum control, which can be adopted for the driving field periodically switched on and off.[66,67] The synthetic inverse temperatures β_S are adjusted by tuning β_L and β_R. Without loss of generality, we randomly initialize the states of the three levels to obtain the mixed-state density matrix of the system and apply the external driving field after the system reaches a steady state.

A. Heat engines, refrigerators, and thermal accelerators

We first discuss how to synthesize the bath at negative inverse temperature. For the given qutrit system, two methods can be employed to obtain continuous synthetic inverse temperatures β_S, namely, by fixing the inverse temperature of the left bath $\beta_L = 0.03$ and adjusting β_R of the right bath from 0.125 down to 0.0125, or by fixing $\beta_R = 0.0375$ while varying β_L from 0.01 to 0.1. The ratio of the two fixed inverse temperatures always equals $E_1 : E_2$. Figures 2(a) and 2(b) show the power and heat fluxes from the left, right, and synthetic baths as functions of the synthetic inverse temperature β_S at a steady state with an external driving field and $\lambda = 5$, $\omega = 9.5$. It is clear that the thermodynamics for various β_S in the two cases are perfectly opposite to each other, so in the following, we solely consider the first case at $\beta_L = 0.03$.

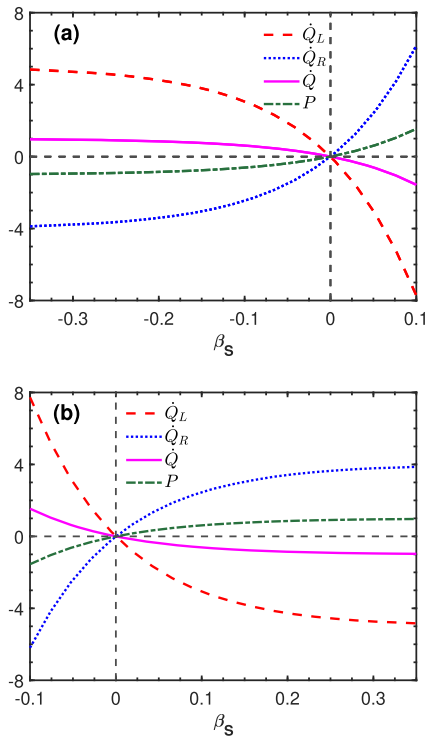

FIG. 2. Power and heat fluxes from the left, right, and synthetic baths as functions of the synthetic inverse temperature β_S at a steady state with an external driving field. (a) For $\beta_L = 0.03$, β_R ranges from 0.125 down to 0.0125 and, thus, $\beta_S \in [-0.35, 0.1]$. (b) For $\beta_R = 0.0375$, β_L increases from 0.01 to 0.1 and $\beta_S \in [-0.1, 0.35]$. The other parameters are $\lambda = 5$ and $\omega = 9.5$.

Building upon the synthetic bath with tunable inverse temperature, the external driving field induces multiple functionalities of the quantum thermal device. As shown in Fig. 2(a), $\dot{Q}_L$ and $\dot{Q}$ decrease from positive to negative values, while $\dot{Q}_R$ and P increase from negative to positive, with β_S ranging from −0.35 to 0.1. It is found that $\dot{Q}_L$, $\dot{Q}_R$, $\dot{Q}$, and P approach zero when $\beta_S = 0$ because the temperature of the synthetic bath tends to infinity. When $\beta_S < 0$, the heat flowing from the left bath to the qutrit system is larger than that from the qutrit to the right bath. As a result, a net heat flow is generated from the synthetic bath into the qutrit, and there could be work that is held by the donor–acceptor molecule, namely, the energy-carrying molecule that plays the role of work repository, which is, subsequently, able to be transferred to some external substance. When $\beta_S > 0$, the heat is transferred from the right bath and dumped into the left bath, passing through the qutrit, and the heat from the right bath surpasses that into the left. Subsequently, sustained net heat flows from the qutrit into the synthetic bath, accompanied by work performed on the device by the external field. It is clear that the directions of $\dot{Q}_L$, $\dot{Q}_R$, $\dot{Q}$, and P for $\beta_S < 0$ are opposite to those for $\beta_S > 0$, respectively. The first law is respected at a steady state as $\dot{Q} + P = 0$. The heat from (into) the left bath consistently exceeds that into (from) the right. For $\beta_S < 0$, $\beta_R > 0.0375$ indicates that the left bath is hotter than the right bath, where the device operates as a heat engine. When $\beta_S > 0$, the right bath may be colder than the left bath for $0 < \beta_S < 0.03$ (i.e., $0.03 < \beta_R < 0.0375$) or hotter than the left for $\beta_S > 0.03$ (i.e., $\beta_R < 0.03$). The device can then be regarded as a refrigerator in the former case or a thermal accelerator in the latter, which is solely a consequence of quantum coherence. The rich phases of the quantum thermal device can be identified by the temperature of the synthetic bath and the temperature differences between the left and right baths.

To comprehend these dynamic phases for both negative and positive β_S, in Fig. 3, we plot the time evolution of the populations and energy transfer for $\lambda = 5$ and $\omega = 9.5$. Figure 3(a) displays the populations of the states $|0\rangle$, $|1\rangle$, and $|2\rangle$ vs time t at $\beta_S = -0.35$. Due to the random initial population distribution across the three levels, there are differences in the rates at which the system reaches a steady state. If the initial population distribution is close to the population required for achieving β_S, the system quickly reaches the target effective temperature. Otherwise, the system takes longer to obtain a steady-state population. When t increases to 10, the system can reach its first steady state in the absence of the external drive, with nearly unchanged populations. At the first steady state, the population of state $|0\rangle$ is the largest of the three, and the population inversion for the states $|1\rangle$ and $|2\rangle$ occurs with the signature of negative temperature. The external driving field is applied since $t = 10$, and then the populations of the three states show underdamped oscillation. The population of state $|0\rangle$ reduces, and the three populations ultimately reach steady-state values. The population difference between the states $|1\rangle$ and $|2\rangle$ becomes smaller in the second steady state compared to that of the first one. Figure 3(b) describes the populations of the states $|0\rangle$, $|1\rangle$, and $|2\rangle$ vs time t at $\beta_S = 0.02$. At the first steady state, the population of the state $|1\rangle$ exceeds that of the state $|2\rangle$ at positive β_S. Once the external driving is turned on for $t \geq 10$, the system reaches the steady state again after the underdamped oscillation. In Fig. 3(c), $\dot{Q}_L$, $\dot{Q}_R$, $\dot{Q}$, and P vs time t are shown at $\beta_S = -0.35$. When t evolves to 10, energy transfer ceases without the external drive, maintaining a thermodynamic

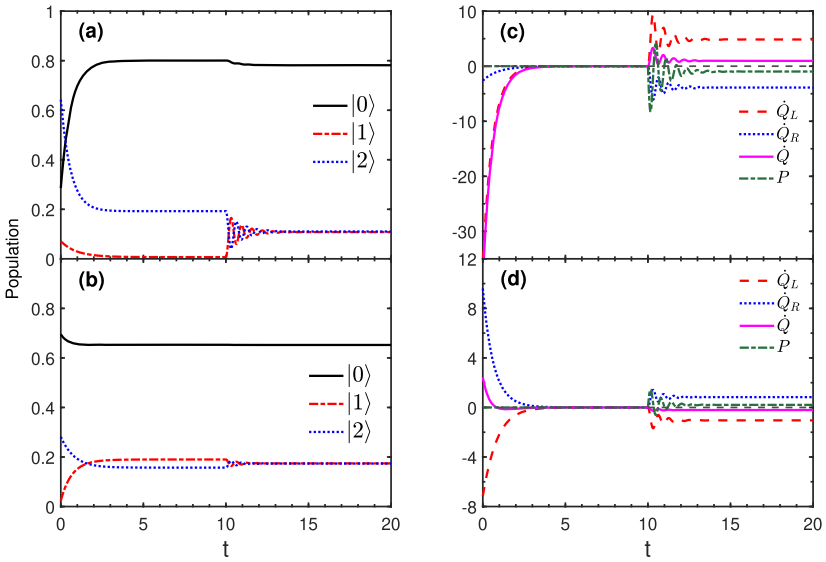

FIG. 3. Time evolution of the populations (a) for $\beta_S = -0.35$ and (b) for $\beta_S = 0.02$. Time evolution of power and heat fluxes from the left, right, and synthetic baths (c) for $\beta_S = -0.35$ as a heat engine and (d) for $\beta_S = 0.02$ as a refrigerator. The external driving field is switched on when $t \geq 10$. The other parameters are $\lambda = 5$ and $\omega = 9.5$.

equilibrium state. Under the action of the driving field, $\dot{Q}_L$, $\dot{Q}_R$, $\dot{Q}$, and P exhibit underdamped responses and then reach steady-state values. Figure 3(d) depicts $\dot{Q}_L$, $\dot{Q}_R$, $\dot{Q}$, and P vs time t at $\beta_S = 0.02$. When the system reaches the second steady state, $\dot{Q}_L$, $\dot{Q}_R$, $\dot{Q}$, and P keep nearly unchanged, indicating persistent net energy transfer. Adjusting the synthetic bath temperature results in the thermal device going through distinct operational modes, each characterized by distinct steady-state energy flux patterns, transient dynamics, and state population distributions.

B. Entropy in quantum thermal devices

In classical thermal devices, the thermodynamic entropy is definitely an essential quantity that needs to be concretely examined. In our model, we, therefore, calculate the entropy fluxes from left and right baths and entropy change rate as functions of the synthetic inverse temperature β_S at a steady state with an external driving field for $\lambda = 5$ and $\omega = 9.5$, as shown in Fig. 4(a). When β_S ranges from -0.35 to 0.1, $\dot{S}_L$ decreases from positive to negative and $\dot{S}_R$ increases inversely. At $\beta_S = 0$, the net entropy flow disappears with the temperature of the synthetic bath going to infinity. The entropy change rate $\dot{S}$ remains vanishing for various β_S, implying no net entropy generation within the system at a steady state. The directions of $\dot{S}_L$ and $\dot{S}_R$ for $\beta_S < 0$ are opposite to that for $\beta_S > 0$, respectively. For $\beta_S < 0$, the entropy is transferred from the left bath into the right bath through the qutrit, and the reverse holds. When $\beta_S \neq 0$, the entropy flowing into the right (left) bath from the qutrit exceeds that into the qutrit from the left (right) bath. In Fig. 4(b), the time evolution of the entropy fluxes from the left and right baths and the entropy change rate are further exhibited for $\beta_S = -0.35$. When t increases to 10, the system can reach thermodynamic equilibrium with $\dot{S}_L$, $\dot{S}_R$, and $\dot{S}$ all equal to zero. For $t \geq 10$, the driving field induces the underdamped oscillations of $\dot{S}_L$, $\dot{S}_R$, and $\dot{S}$, culminating in the establishment of the second steady state. Figure 4(c) displays $\dot{S}_L$, $\dot{S}_R$, and $\dot{S}$ vs time t for $\beta_S = 0.02$. Due to the external drive, the first steady state of the system is followed by underdamped responses of $\dot{S}_L$, $\dot{S}_R$, and $\dot{S}$. When the system reaches the second steady state, $\dot{S}_L$ and $\dot{S}_R$ stabilize at their respective values, implying constant net entropy fluxes.

Beyond analyzing the entropy flux between the qutrit and the baths, the von Neumann entropy of the three-level system also warrants close scrutiny. Figure 5(a) shows the entropy of the qutrit system as a function of the synthetic inverse temperature β_S at a steady state for $\lambda = 0$ and $\lambda = 5$ with $\omega = 9.5$. At $\beta_S = 0$, the temperature of the synthetic bath tends to infinity. For $\lambda = 0$ and $\lambda = 5$, entropies increase when β_S ranges from negative to positive values. Note that the entropy depends on the population distribution among all three levels, and we have defined the temperature for a reduced two-level subsystem using the relevant ratio of populations.[68] This explains the monotonic behavior observed here as opposed to the nonmonotonic trend reported in Ref. 34, in which the definition of temperature follows the usual thermodynamic fashion as $\beta = \partial S/\partial E$. For $\lambda = 0$, the external drive is absent and the interaction between the qutrit and the two baths holds. As β_R of the right bath falls from 0.125 to 0.0125 at $\beta_L = 0.03$, the right bath heats up and raises the entropy of the qutrit system. At $\lambda = 5$, the external drive appears to enhance the hybridization of the three levels, so the entropy for $\lambda = 5$ is higher than that for $\lambda = 0$, and the energy could be more reposited. The time evolution of the entropy of the three-level system for various β_S at $\omega = 9.5$ in Fig. 5(b) is as expected. When t evolves to 10, the qutrit system and two baths reach thermal equilibrium. For $\beta_S = 0$, the entropy remains nearly unchanged upon the introduction of the external drive, meaning it can be ignored. When $\beta_S = -0.35$ and $\beta_S = 0.02$, S experiences an increase in response to the external drive. After the external driving field is switched on, the increase in the entropy is attributed to the reduction in the population difference between the states $|1\rangle$ and $|2\rangle$. When t increases to 20, S remains nearly unchanged, implying the establishment of a steady state.

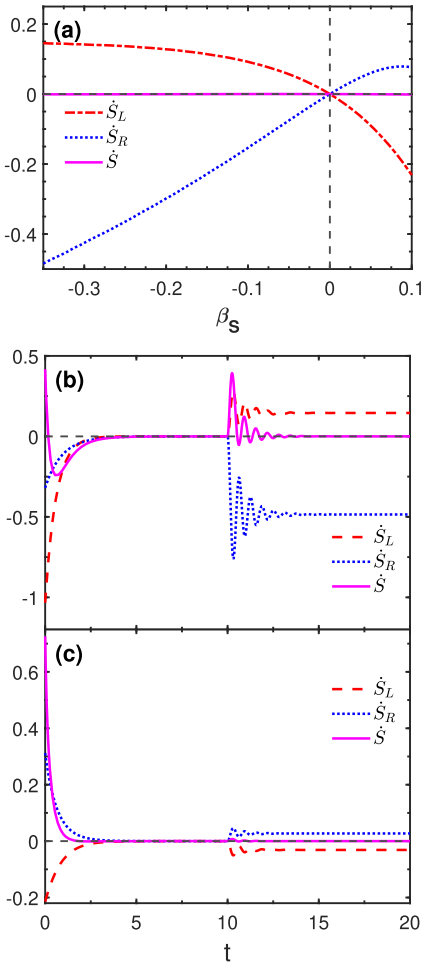

FIG. 4. (a) The entropy fluxes from left and right baths and entropy change rate as functions of the synthetic inverse temperature β_S at a steady state with an external drive. Time evolution of the entropy fluxes from left and right baths and entropy change rate (b) for $\beta_S = -0.35$ as a heat engine and (c) for $\beta_S = 0.02$ as a refrigerator. The external driving field is switched on when $t \geq 10$. The other parameters are $\lambda = 5$ and $\omega = 9.5$.

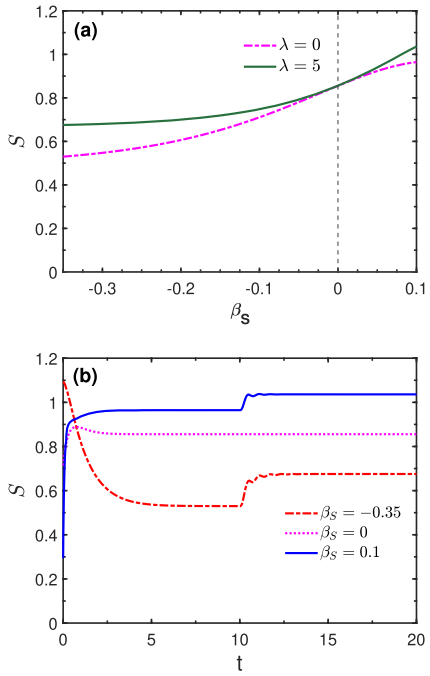

FIG. 5. (a) Entropy of the qutrit system as a function of the synthetic inverse temperature β_S at a steady state for various values of λ with $\omega = 9.5$. (b) Time evolution of the entropy for various values of β_S at $\omega = 9.5$. The external driving field is switched on when $t \geq 10$.

C. The counter-rotating component of the driving field

In order to go beyond the performance of classical thermal devices, we now focus on the effect of the external driving field on the power of the device. The power P as a function of λ at a steady state for various β_S with $\omega = 9.5$ is displayed in Fig. 6(a). When $\lambda = 0$, the influence of the external drive can be neglected, so $P = 0$. With λ increasing, the power decreases for negative β_S and increases for positive β_S. For small λ (e.g., $\lambda < 1$), the power exhibits significant variation with λ increasing from zero, but the power is saturated for large λ (e.g., $\lambda > 2$). Figure 6(b) shows the power P as a function of ω at a steady state for various β_S with $\lambda = 5$. When $\omega = 0$, the driving field can be treated as a static electromagnetic field leading to no interaction-free qutrit, so that $P = 0$. The external field for negative frequencies corresponds to the counter-rotating wave terms of the driving interaction, which have been typically neglected under the rotating wave approximation.[46,47] However, the counter-rotating wave terms have been extensively discussed across a range of literature and shown to play an important role in various aspects of quantum dynamics.[69–74] It is worth considering how the counter-rotating component of the driving field, which has become dominant, impacts the energy flow. Given specific β_S, the direction of P for negative ω is opposite to that for positive ω since the thermodynamics for opposite ω can be regarded as time reversal processes.

Most importantly, since in the rotating-wave frame, the symmetry in the frequency domain of the full Rabi model is broken, the power with positive and negative frequency exhibits a significant difference. To this end, we further study the negative-frequency domain by plotting the power and the heat fluxes from the left, right, and synthetic baths vs time t in Fig. 6(c). At the second steady state, the heat flowing into the cold right bath is larger than that from the hot left one. The work is performed on the device by the driving field, and thus, the device acts as a thermal accelerator. Figure 6(d) exhibits the power and the heat fluxes from the left, right, and synthetic baths vs time t for $\omega = -9.5$, $\beta_S = 0.02$, and $\lambda = 5$. It is observed that the directions of $\dot{Q}_L$ and $\dot{Q}_R$ for a given β_S remain consistent at a steady state, regardless of whether ω is positive or negative. When the system reaches the second steady state, a net heat flows from the cold right bath to the hot left bath through the qutrit, and the work is reposited and then transferred to the external substance, acting like a thermal ratchet. This behavior of energy flow

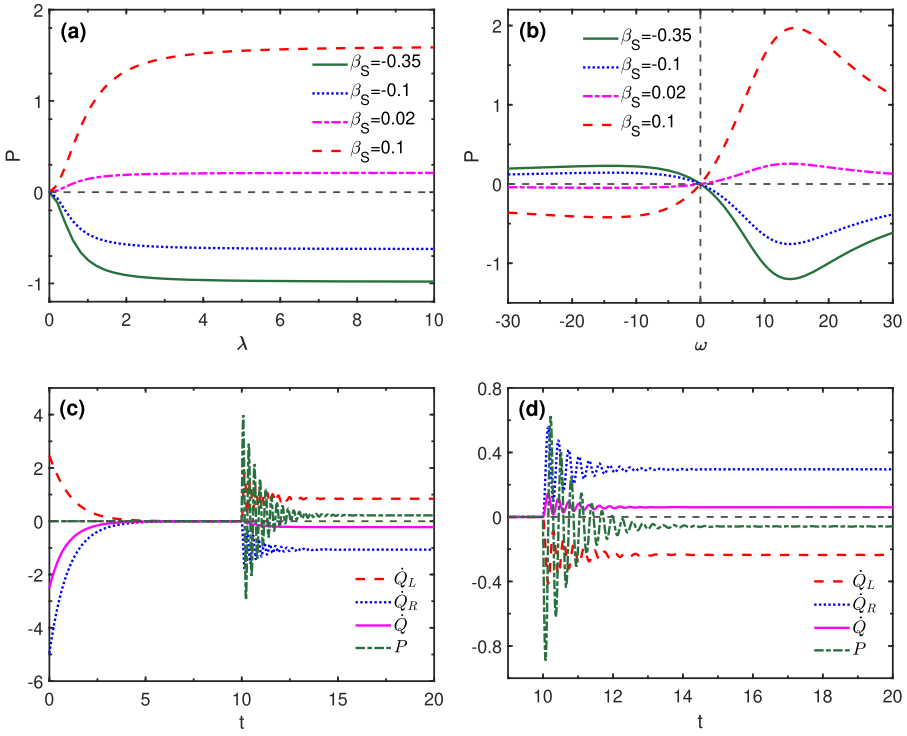

FIG. 6. (a) Power vs λ at a steady state for various β_S with $\omega = 9.5$. (b) Power vs ω at a steady state for various β_S with $\lambda = 5$. Time evolution of the power and heat fluxes from the left, right, and synthetic baths (c) for $\beta_S = -0.35$ as a thermal accelerator and (d) for $\beta_S = 0.02$ as a thermal ratchet. The other parameters are $\omega = -9.5$ and $\lambda = 5$. The external driving field is switched on when $t \geq 10$.

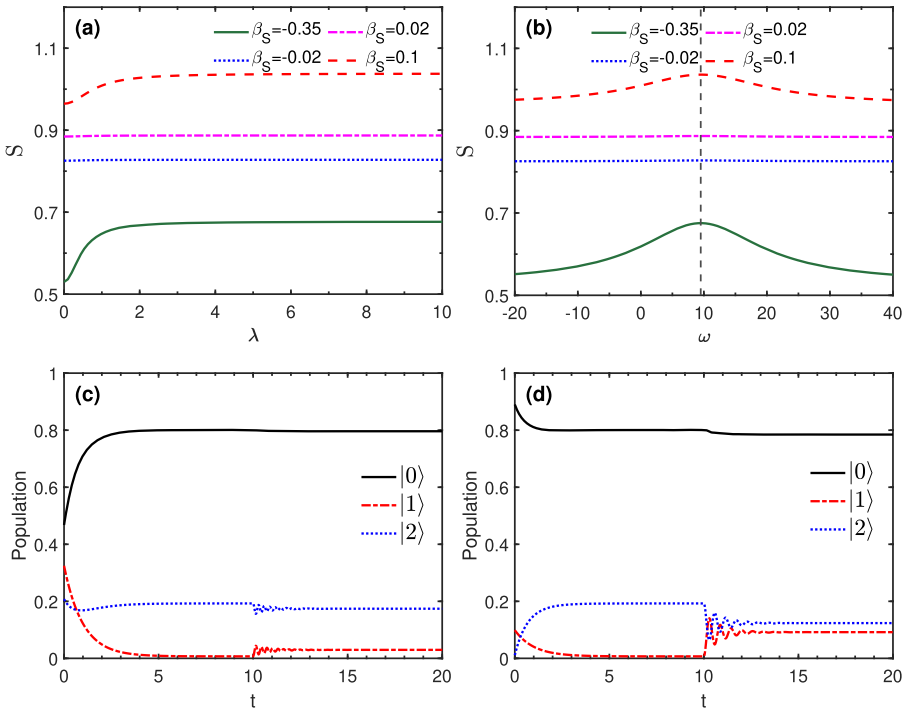

FIG. 7. (a) Entropy vs λ at a steady state for various β_S at $\omega = 9.5$. (b) Entropy vs ω at a steady state for various β_S at $\lambda = 5$. Time evolution of the populations of the three levels (c) for $\omega = -9.5$ and (d) for $\omega = 14$. The other parameters are $\beta_S = -0.35$ and $\lambda = 5$.

can be attributed to time reversal effects induced by the driving field with negative frequency. The value of power is equal to the value of the reduced heat flux from the right to the left bath, implying that all the output work externally originates from the heat, with no energy being transferred from the driving field. In addition, supposing the idealized cold right bath can always provide the necessary heat input for the device to function, the first law of thermodynamics is respected. Overall, by incorporating the negative frequency regime of the driving field, the quantum thermal device transitions seamlessly among the refrigerator, thermal accelerator, thermal ratchet, and heat engine phases.

One may now be wondering about the behavior of entropy for negative ω. Figure 7(a) shows the entropy S as a function of λ at a steady state for various β_S at $\omega = 9.5$. For $\beta_S = -0.02$ and $\beta_S = 0.02$, the temperature of the synthetic bath is high enough that the external drive can hardly influence the entropy of the three-level system, so S experiences little increase as λ increases. For $\beta_S = -0.35$ and $\beta_S = 0.1$, S increases with λ. For large λ (e.g., $\lambda > 2$), the coupling strength is too large to induce saturation of the entropy. Figure 7(b) shows the entropy S as a function of ω at a steady state for various β_S at $\lambda = 5$. For $\beta_S = -0.02$ and $\beta_S = 0.02$, again, the temperature of the synthetic bath is sufficiently high, so S exhibits little variation. For $\beta_S = -0.35$ and $\beta_S = 0.1$, the entropy reaches its peak at $\omega = 9.5$. At this frequency, the external driving field reaches resonance of the levels $|1\rangle$ and $|2\rangle$, where the population difference of the two levels decreases to its minimum [as shown in Figs. 3(a) and 3(b)]. Figure 7(c) also displays in the negative-frequency domain the populations of the three levels vs time t at $\omega = -9.5$ for $\beta_S = -0.35$ and $\lambda = 5$. When the system reaches the second steady state after underdamped oscillation, the population difference between $|1\rangle$ and $|2\rangle$ is remarkable. Figure 7(d) depicts the populations of the three levels vs time t at $\omega = 14$ for $\beta_S = -0.35$ and $\lambda = 5$. At the second steady state, the notable population difference between $|1\rangle$ and $|2\rangle$ indicates the system is in the detuning condition. In brief, the change of entropy becomes complicated in this situation.

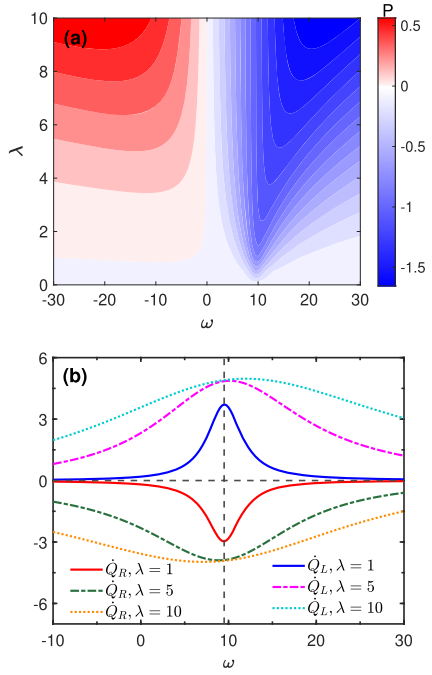

FIG. 8. (a) Contour plots of power P as a function of the driving field parameters ω and λ at $\beta_S = -0.35$. (b) The heat fluxes from the left and right baths as functions of ω at a steady state for various λ with $\beta_S = -0.35$.

To further clarify the dependence of the power on ω and λ, especially the sign of frequency, we plot another phase diagram of the power P as a function of ω and λ at $\beta_S = -0.35$ in Fig. 8(a). When $\omega(\lambda) \to 0$ or $\omega \to \pm\infty$, the power tends to zero because of the negligible influence of the external drive. For a given λ, there exist values of ω where the power takes its positive maximal value and negative minimal value. With λ decreasing, the frequency with respect to the minimal value of power for $\omega > 0$ tends to be 9.5. Figure 8(b) displays the heat fluxes from the left and right baths as functions of ω for various λ at $\beta_S = -0.35$. When $\omega \to \pm\infty$, $\dot{Q}_L$ and $\dot{Q}_R$ tend to zero. For small λ (e.g., $\lambda = 1$), ω takes 9.5 for $\dot{Q}_L$ taking its positive maximal value, and $\dot{Q}_R$ taking its negative minimal value. For large λ (e.g., $\lambda = 5$ and $\lambda = 10$), the frequency corresponding to the maximal value of $\dot{Q}_L$ blue shifts and that to the minimal value of $\dot{Q}_R$ red shifts with λ increasing. The rotating and counter-rotating components of the driving field exert distinctly different influences on the energy flow within the quantum thermal device.

D. Relating to a real thermal device

We now turn to discuss the external driving field that is subjected to a periodic modulation, wherein it is alternately switched on and off in terms of a predefined temporal pattern, which can be easily realized in practice by designing the microwave sequences well. At the initial moment, the external drive is deactivated, and the system reaches thermal equilibrium after a period of t_0 with the two baths. Subsequently, the external driving field is periodically switched on and off, where the field strength has a periodic time dependence modeled by

$$\lambda(t) = \begin{cases} \lambda_0 & \text{if } [(t - t_0) \bmod T] < t_{\text{on}}, \\ 0 & \text{if } t_{\text{on}} \le [(t - t_0) \bmod T] < T, \end{cases} \tag{11}$$

with t_{on} and t_{off} representing the duration of the application and removal of the external driving field, respectively, within each cycle, $T = t_{\text{on}} + t_{\text{off}}$. The work is then defined by

$$W = \int_{t_0}^{t} \text{Tr}\left[\rho(t')\frac{\partial H(t')}{\partial t'}\right] dt', \tag{12}$$

and the average power is given by

$$\tilde{P} = \frac{1}{t - t_0}\int_{t_0}^{t} \text{Tr}\left[\rho(t')\frac{\partial H(t')}{\partial t'}\right] dt'. \tag{13}$$

Negative $\tilde{P}$ implies that the net work is reposited and transferred to an external substance, while positive $\tilde{P}$ indicates the reverse.

The periodic modulation of the driving field, achieved through systematic on–off cycles, facilitates a detailed investigation of the transient responses of quantum thermal devices. In Fig. 9(a), we plot the populations of the three levels vs time t with the external

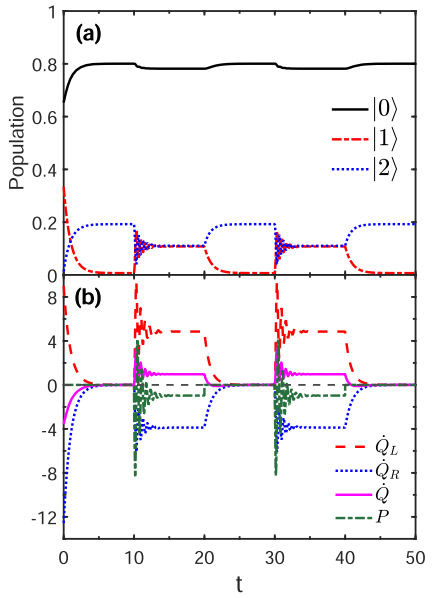

FIG. 9. (a) Time evolution of the populations with the external driving field switched on and off periodically for $t_{on} = 10$ and $t_{off} = 10$. (b) Time evolution of the power and the heat fluxes from the left, right, and synthetic baths with the external driving field switching on and off periodically at every $t = 10$. The other parameters are $\beta_S = -0.35$, $\lambda_0 = 5$, and $\omega = 9.5$.

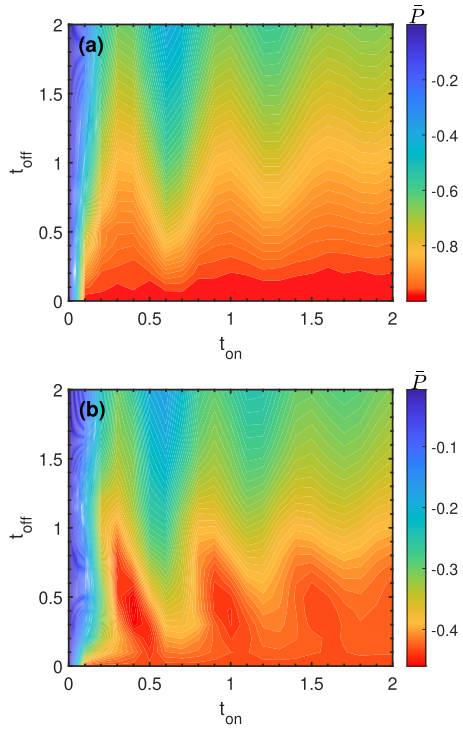

FIG. 10. Contour plots of the average power $\bar{P}$ as a function of t_{on} and t_{off} (a) for $\omega = 9.5$ and (b) for $\omega = 5$. The other parameters are $\beta_S = -0.35$ and $\lambda_0 = 5$.

drive switched on and off periodically for every $t = 10$. The external drive is removed since $t = 20$, with the population of $|1\rangle$ decreasing and the populations of $|0\rangle$ and $|2\rangle$ increasing. The population difference between $|1\rangle$ and $|2\rangle$ increases, and the populations can be fully recovered to their equilibrium values after the entire time evolution, manifesting the time reversibility. In Fig. 9(b), we plot the power and the heat fluxes from the left, right, and synthetic baths vs time t with the external drive switched on and off periodically for $t_{on} = 10$ and $t_{off} = 10$. The external driving field is applied again since $t = 30$, leading to underdamped responses of $\dot{Q}_L$, $\dot{Q}_R$, $\dot{Q}$, and P. The thermodynamic processes are completely repeated as those when the external driving is first applied.

To get insight into the dependence of the average power on t_{on} and t_{off}, we show a phase diagram of $\bar{P}$ as a function of t_{on} and t_{off} in Fig. 10(a) for $\omega = 9.5$, $\beta_S = -0.35$, and $\lambda_0 = 5$. When $t_{on} \to 0$, the average power tends to zero, where the external drive can be ignored. When $t_{off} = 0$ and t_{on} is considerable (e.g., $t_{on} > 0.1$), the work is reposited and delivered to the external substance with identical maximum average power for various values of t_{on}. For a certain t_{on}, the average power increases as t_{off} expands since the device cannot perform work when the external drive is removed, leading to a decrease in the total work transferred to the external one. For a given t_{off} (e.g., $t_{off} > 0.1$), the average power fluctuates with t_{on} increasing from zero, and the optimal t_{on} can facilitate the average power. Figure 10(b) shows a phase diagram of $\bar{P}$ as a function of t_{on} and t_{off} for $\omega = 5$, $\beta_S = -0.35$, and $\lambda_0 = 5$. When $t_{off} = 0$ and $t_{on} > 0.2$, the average power remains unchanged with t_{on} increasing. For a given t_{on} (e.g., $t_{on} = 0.4$), the average power for small t_{off} (e.g., $t_{off} = 0.4$) can be less negative than that for $t_{off} = 0$. For the optimized t_{on} and t_{off}, the net work repository can exceed that at a steady state.

We define the average power difference as

$$\Delta\bar{P} = \bar{P}_0 - \bar{P}, \tag{14}$$

where $\bar{P}_0$ denotes the average power with $t_{off} = 0$ and the same t_{on} as that for $\bar{P}$. The average power difference $\Delta\bar{P} < 0$ indicates more work that can be delivered to the external compared to that at steady state conditions, while $\Delta\bar{P} > 0$ for the inverse. Figure 11(a) displays $\Delta\bar{P}$ as a function of t_{on} for various ω at $t_{off} = 0.4$ with $\beta_S = -0.35$ and $\lambda_0 = 5$. For $\omega = 7$ and $\omega = 12$, $\Delta\bar{P}$ fluctuates as positive values when $t_{on} > 0$. When $\omega = 5$ and $\omega = 14$, $\Delta\bar{P}$ can reach negative values for specific t_{on} (e.g., $t_{on} = 0.4$). Figure 11(b) depicts the power and the heat fluxes from the left, right, and synthetic baths vs time t for $\omega = 5$, $t_{on} = 0.4$, and $t_{off} = 0.4$. When the external drive is turned on and off periodically, $\dot{Q}_L$, $\dot{Q}_R$, $\dot{Q}$, and P exhibit cyclical variations, while when it is removed, the power remains vanishing, indicating the device does not perform work. The power fluctuates with predominantly negative values, representing the underdamped response of the system in an unsteady state whenever the external drive is activated. Figure 11(c) shows the work W vs time t at $t_{on} = 0.4$ for various ω and t_{off}. As t_{off} grows to 10, the external drive is switched off, leading to vanishing W and no output work. When $t_{off} = 0$, W continuously reduces in the second steady state for $\omega = 5$ and $\omega = 9.5$, and when $t_{off} = 0.4$, W decreases upon the activation of the external drive and remains unchanged when the external drive is switched off. Despite

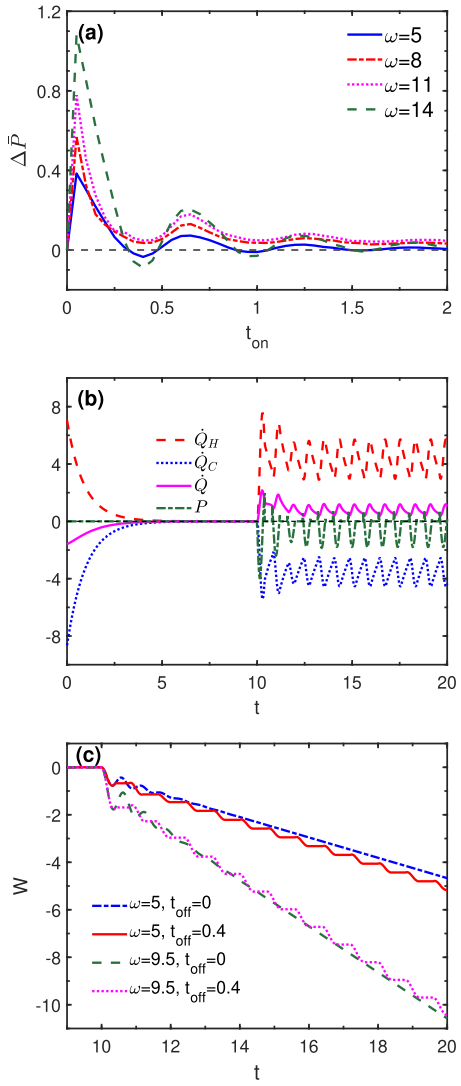

FIG. 11. (a) Average power difference $\Delta\bar{P}$ as a function of t_{on} for various ω at $t_{off} = 0.4$. (b) Time evolution of power and heat fluxes from the left, right, and synthetic baths for $\omega = 5$ and $t_{on} = 0.4$. (c) Time evolution of work W for various ω and t_{on}. The other parameters are $\beta_S = -0.35$ and $\lambda_0 = 5$.

the presence of multiple step-like lineshapes, W exhibits a more substantial decrease for $t_{off} = 0.4$ than that for $t_{off} = 0$. Consequently, the device under large detuning conditions in an unsteady state can do more net work than in a steady state.

IV. CONCLUSION

In summary, we employ a three-level system to simulate the dynamic phases of various functions in an energy-carrying molecular thermal device. From the dynamic viewpoint, these phases manifest varying directions of heat and work flow, which depend on the temperature of the synthetic bath and the frequency of the external driving field. We found that the direction of the energy transfer reverses with the sign of synthetic temperature β_S; that is, the device can be operated as a heat engine, refrigerator, or thermal accelerator at various values of β_S. Subject to the thermalization of the whole system, the underdamped response occurs after the external driving field is enforced. Introducing the external drive in thermodynamic equilibrium can enhance the von Neumann entropy of the three-level system, which is lower for the bath at negative temperatures than that at positive temperatures. At a steady state, the absolute magnitude of power increases with λ increasing and saturates with sufficiently large λ in the rotating-wave frame. The direction of power reverses with the sign of the frequency of the driving field ω, while the direction of net heat transfer remains constant. With the negative frequency of the driving field in terms of rotating waves, the heat can flow from the cold bath to the hot bath, and the work is deposited and can be delivered to the external. The frequency corresponding to the minimal value of power blue shifts for negative β_S. When the external drive is switched on and off periodically, the heat fluxes and power exhibit cyclical variations, manifesting the character of a thermal engine. For negative β_S, the net work repository for output decreases with t_{off} growing at considerable t_{on} in resonant conditions. For some t_{on}, the output work for optimal t_{off} can exceed that for $t_{off} = 0$ with negative β_S under large detuning conditions. Our research delineates a tangible pathway toward the practical deployment of highly efficient molecular thermal devices.

ACKNOWLEDGMENTS

This work was supported by the National Natural Science Foundation of China (Grant No. 12374107).

AUTHOR DECLARATIONS

Conflict of Interest

The authors have no conflicts to disclose.

Author Contributions

Guo-hao Xu: Data curation (lead); Formal analysis (equal); Investigation (lead); Methodology (lead); Visualization (lead); Writing – original draft (lead); Writing – review & editing (equal). **Jiarui Zeng**: Data curation (equal); Formal analysis (equal); Methodology (equal); Validation (equal); Visualization (equal); Writing – review & editing (equal). **Yao Yao**: Conceptualization (lead); Formal analysis (equal); Funding acquisition (lead); Project administration (lead); Supervision (lead); Writing – review & editing (lead).

DATA AVAILABILITY

The data that support the findings of this study are available from the corresponding author upon reasonable request.

REFERENCES

[1] F. Binder, L. A. Correa, C. Gogolin, J. Anders, and G. Adesso, *Thermodynamics in the Quantum Regime: Fundamental Theories of Physics* (Springer, Cham, Switzerland, 2018), Vol. 195.
[2] S. Deffner and S. Campbell, *Quantum Thermodynamics: An Introduction to the Thermodynamics of Quantum Information* (Morgan & Claypool Publishers, 2019).

[3]J. Roßnagel, S. T. Dawkins, K. N. Tolazzi, O. Abah, E. Lutz, F. Schmidt-Kaler, and K. Singer, "A single-atom heat engine," Science **352**, 325–329 (2016).
[4]D. von Lindenfels, O. Gräb, C. T. Schmiegelow, V. Kaushal, J. Schulz, M. T. Mitchison, J. Goold, F. Schmidt-Kaler, and U. G. Poschinger, "Spin heat engine coupled to a harmonic-oscillator flywheel," Phys. Rev. Lett. **123**, 080602 (2019).
[5]G. Maslennikov, S. Ding, R. Hablützel, J. Gan, A. Roulet, S. Nimmrichter, J. Dai, V. Scarani, and D. Matsukevich, "Quantum absorption refrigerator with trapped ions," Nat. Commun. **10**, 202 (2019).
[6]J. Klatzow, J. N. Becker, P. M. Ledingham, C. Weinzetl, K. T. Kaczmarek, D. J. Saunders, J. Nunn, I. A. Walmsley, R. Uzdin, and E. Poem, "Experimental demonstration of quantum effects in the operation of microscopic heat engines," Phys. Rev. Lett. **122**, 110601 (2019).
[7]S. Zaiser, C. T. Cheung, S. Yang, D. B. R. Dasari, S. Raeisi, and J. Wrachtrup, "Cyclic cooling of quantum systems at the saturation limit," npj Quantum Inf. **7**, 92 (2021).
[8]R. R. Soldati, D. B. R. Dasari, J. Wrachtrup, and E. Lutz, "Thermodynamics of a minimal algorithmic cooling refrigerator," Phys. Rev. Lett. **129**, 030601 (2022).
[9]J.-P. Brantut, C. Grenier, J. Meineke, D. Stadler, S. Krinner, C. Kollath, T. Esslinger, and A. Georges, "A thermoelectric heat engine with ultracold atoms," Science **342**, 713–715 (2013).
[10]Q. Bouton, J. Nettersheim, S. Burgardt, D. Adam, E. Lutz, and A. Widera, "A quantum heat engine driven by atomic collisions," Nat. Commun. **12**, 2063 (2021).
[11]A. Roy and A. Eckardt, "Design and characterization of a quantum heat pump in a driven quantum gas," Phys. Rev. E **101**, 042109 (2020).
[12]A. O. Niskanen, Y. Nakamura, and J. P. Pekola, "Information entropic superconducting microcooler," Phys. Rev. B **76**, 174523 (2007).
[13]M. Campisi, J. Pekola, and R. Fazio, "Nonequilibrium fluctuations in quantum heat engines: Theory, example, and possible solid state experiments," New J. Phys. **17**, 035012 (2015).
[14]B. Karimi and J. P. Pekola, "Otto refrigerator based on a superconducting qubit: Classical and quantum performance," Phys. Rev. B **94**, 184503 (2016).
[15]G. Marchegiani, P. Virtanen, F. Giazotto, and M. Campisi, "Self-oscillating Josephson quantum heat engine," Phys. Rev. Appl. **6**, 054014 (2016).
[16]B. Scharf, A. Braggio, E. Strambini, F. Giazotto, and E. M. Hankiewicz, "Topological Josephson heat engine," Commun. Phys. **3**, 198 (2020).
[17]D. Segal and A. Nitzan, "Molecular heat pump," Phys. Rev. E **73**, 026109 (2006).
[18]X. Ding, J. Yi, Y. W. Kim, and P. Talkner, "Measurement-driven single temperature engine," Phys. Rev. E **98**, 042122 (2018).
[19]L. Bresque, P. A. Camati, S. Rogers, K. Murch, A. N. Jordan, and A. Auffèves, "Two-qubit engine fueled by entanglement and local measurements," Phys. Rev. Lett. **126**, 120605 (2021).
[20]K. Zhang, F. Bariani, and P. Meystre, "Quantum optomechanical heat engine," Phys. Rev. Lett. **112**, 150602 (2014).
[21]A. Ü. C. Hardal and Ö. E. Müstecaplıoğlu, "Superradiant quantum heat engine," Sci. Rep. **5**, 12953 (2015).
[22]J. Klaers, S. Faelt, A. Imamoglu, and E. Togan, "Squeezed thermal reservoirs as a resource for a nanomechanical engine beyond the Carnot limit," Phys. Rev. X **7**, 031044 (2017).
[23]H. Terças, S. Ribeiro, M. Pezzutto, and Y. Omar, "Quantum thermal machines driven by vacuum forces," Phys. Rev. E **95**, 022135 (2017).
[24]T. B. Arp, Y. Barlas, V. Aji, and N. M. Gabor, "Natural regulation of energy flow in a green quantum photocell," Nano Lett. **16**, 7461–7466 (2016).
[25]A. Singh and C. Benjamin, "Magic angle twisted bilayer graphene as a highly efficient quantum Otto engine," Phys. Rev. B **104**, 125445 (2021).
[26]N. Killoran, S. F. Huelga, and M. B. Plenio, "Enhancing light-harvesting power with coherent vibrational interactions: A quantum heat engine picture," J. Chem. Phys. **143**, 155102 (2015).
[27]F. J. Peña, D. Zambrano, O. Negrete, G. De Chiara, P. A. Orellana, and P. Vargas, "Quasistatic and quantum-adiabatic Otto engine for a two-dimensional material: The case of a graphene quantum dot," Phys. Rev. E **101**, 012116 (2020).
[28]H. E. D. Scovil and E. O. Schulz-DuBois, "Three-level masers as heat engines," Phys. Rev. Lett. **2**, 262 (1959).
[29]E. M. Purcell and R. V. Pound, "A nuclear spin system at negative temperature," Phys. Rev. **81**, 279 (1951).
[30]M. Baldovin, S. Iubini, R. Livi, and A. Vulpiani, "Statistical mechanics of systems with negative temperature," Phys. Rep. **923**, 1–50 (2021).
[31]S. Hilbert, P. Hänggi, and J. Dunkel, "Thermodynamic laws in isolated systems," Phys. Rev. E **90**, 062116 (2014).
[32]H. Struchtrup, "Work storage in states of apparent negative thermodynamic temperature," Phys. Rev. Lett. **120**, 250602 (2018).
[33]M. L. Bera, T. Pandit, K. Chatterjee, V. Singh, M. Lewenstein, U. Bhattacharya, and M. N. Bera, "Steady-state quantum thermodynamics with synthetic negative temperatures," Phys. Rev. Res. **6**, 013318 (2024).
[34]N. F. Ramsey, "Thermodynamics and statistical mechanics at negative absolute temperatures," Phys. Rev. **103**, 20 (1956).
[35]H. P. Goswami and U. Harbola, "Thermodynamics of quantum heat engines," Phys. Rev. A **88**, 013842 (2013).
[36]H. Zhou, J. Thingna, J.-S. Wang, and B. Li, "Thermoelectric transport through a quantum nanoelectromechanical system and its backaction," Phys. Rev. B **91**, 045410 (2015).
[37]J. Onam González, D. Alonso, and J. P. Palao, "Performance of continuous quantum thermal devices indirectly connected to environments," Entropy **18**, 166 (2016).
[38]R. Silva, G. Manzano, P. Skrzypczyk, and N. Brunner, "Performance of autonomous quantum thermal machines: Hilbert space dimension as a thermodynamical resource," Phys. Rev. E **94**, 032120 (2016).
[39]T. Feldmann and R. Kosloff, "Performance of discrete heat engines and heat pumps in finite time," Phys. Rev. E **61**, 4774 (2000).
[40]A. A. S. Kalaee and A. Wacker, "Positivity of entropy production for the three-level maser," Phys. Rev. A **103**, 012202 (2021).
[41]M. Qutubuddin and K. E. Dorfman, "Incoherent control of two-photon induced optical measurements in open quantum systems: Quantum heat engine perspective," Phys. Rev. Res. **4**, 023259 (2022).
[42]J. P. Gordon, H. J. Zeiger, and C. H. Townes, "The maser—New type of microwave amplifier, frequency standard, and spectrometer," Phys. Rev. **99**, 1264 (1955).
[43]D. Kleppner, H. M. Goldenberg, and N. F. Ramsey, "Theory of the hydrogen maser," Phys. Rev. **126**, 603 (1962).
[44]J. E. Geusic, E. O. Schulz-DuBios, and H. E. D. Scovil, "Quantum equivalent of the Carnot cycle," Phys. Rev. **156**, 343 (1967).
[45]N. Bloembergen, "Proposal for a new type solid state maser," Phys. Rev. **104**, 324 (1956).
[46]E. Boukobza and D. J. Tannor, "Three-level systems as amplifiers and attenuators: A thermodynamic analysis," Phys. Rev. Lett. **98**, 240601 (2007).
[47]A. A. S. Kalaee, A. Wacker, and P. P. Potts, "Violating the thermodynamic uncertainty relation in the three-level maser," Phys. Rev. E **104**, L012103 (2021).
[48]B. Mohan, R. Gangwar, T. Pandit, M. L. Bera, M. Lewenstein, and M. N. Bera, "Coherent heat transfer leads to genuine quantum enhancement in performances of continuous engines," arXiv:2404.05799 [quant-ph] (2024).
[49]R. Uzdin, A. Levy, and R. Kosloff, "Equivalence of quantum heat machines, and quantum-thermodynamic signatures," Phys. Rev. X **5**, 031044 (2015).
[50]B. K. Rugg, M. D. Krzyaniak, B. T. Phelan, M. A. Ratner, R. M. Young, and M. R. Wasielewski, "Photodriven quantum teleportation of an electron spin state in a covalent donor–acceptor–radical system," Nat. Chem. **11**, 981–986 (2019).
[51]M. Atzori, L. Tesi, E. Morra, M. Chiesa, L. Sorace, and R. Sessoli, "Room-temperature quantum coherence and Rabi oscillations in vanadyl phthalocyanine: Toward multifunctional molecular spin qubits," J. Am. Chem. Soc. **138**, 2154–2157 (2016).
[52]Y. Qiu, H. J. Eckvahl, A. Equbal, M. D. Krzyaniak, and M. R. Wasielewski, "Enhancing coherence times of chromophore-radical molecular qubits and qudits by rational design," J. Am. Chem. Soc. **145**, 25903–25909 (2023).
[53]E. Collini, "Spectroscopic signatures of quantum-coherent energy transfer," Chem. Soc. Rev. **42**, 4932–4947 (2013).
[54]G. D. Scholes, G. R. Fleming, L. X. Chen, A. Aspuru-Guzik, A. Buchleitner, D. F. Coker, G. S. Engel, R. Van Grondelle, A. Ishizaki, D. M. Jonas *et al.*, "Using coherence to enhance function in chemical and biophysical systems," Nature **543**, 647–656 (2017).

[55]K. E. Dorfman, D. V. Voronine, S. Mukamel, and M. O. Scully, "Photosynthetic reaction center as a quantum heat engine," Proc. Natl. Acad. Sci. U. S. A. **110**, 2746–2751 (2013).
[56]H.-P. Breuer and F. Petruccione, *The Theory of Open Quantum Systems* (Oxford University Press, 2002).
[57]L. Buffoni, A. Solfanelli, P. Verrucchi, A. Cuccoli, and M. Campisi, "Quantum measurement cooling," Phys. Rev. Lett. **122**, 070603 (2019).
[58]F. Zhan, N. Li, S. Kohler, and P. Hänggi, "Molecular wires acting as quantum heat ratchets," Phys. Rev. E **80**, 061115 (2009).
[59]S. Yukawa, M. Kikuchi, G. Tatara, and H. Matsukawa, "Quantum ratchets," J. Phys. Soc. Jpn. **66**, 2953–2956 (1997).
[60]M. Born, *Atomic Physics* (Blackie, 1944).
[61]R. Alicki, "The quantum open system as a model of the heat engine," J. Phys. A: Math. Gen. **12**, L103 (1979).
[62]R. Kosloff, "A quantum mechanical open system as a model of a heat engine," J. Chem. Phys. **80**, 1625–1631 (1984).
[63]E. Geva, R. Kosloff, and J. L. Skinner, "On the relaxation of a two-level system driven by a strong electromagnetic field," J. Chem. Phys. **102**, 8541–8561 (1995).
[64]R. Kosloff and T. Feldmann, "Discrete four-stroke quantum heat engine exploring the origin of friction," Phys. Rev. E **65**, 055102 (2002).
[65]E. Boukobza and D. J. Tannor, "Thermodynamics of bipartite systems: Application to light-matter interactions," Phys. Rev. A **74**, 063823 (2006).
[66]A. R. Milne, C. Hempel, L. Li, C. L. Edmunds, H. J. Slatyer, H. Ball, M. R. Hush, and M. J. Biercuk, "Quantum oscillator noise spectroscopy via displaced cat states," Phys. Rev. Lett. **126**, 250506 (2021).
[67]H. Levine, A. Keesling, A. Omran, H. Bernien, S. Schwartz, A. S. Zibrov, M. Endres, M. Greiner, V. Vuletić, and M. D. Lukin, "High-fidelity control and entanglement of Rydberg-atom qubits," Phys. Rev. Lett. **121**, 123603 (2018).
[68]E. Abraham and O. Penrose, "Physics of negative absolute temperatures," Phys. Rev. E **95**, 012125 (2017).
[69]C. Zhao and H. Zheng, "Interference between driving and dissipation in the spin-boson model: Effect of counter-rotating terms," Phys. Rev. A **82**, 043844 (2010).
[70]W. Wu and M. Liu, "Effects of counter-rotating-wave terms on the non-Markovianity in quantum open systems," Phys. Rev. A **96**, 032125 (2017).
[71]Z.-Z. Zhang and W. Wu, "Effects of counter-rotating-wave terms on the noisy frequency estimation," Phys. Rev. A **105**, 043706 (2022).
[72]C. Wang and Q.-H. Chen, "Exact dynamics of quantum correlations of two qubits coupled to bosonic baths," New J. Phys. **15**, 103020 (2013).
[73]Y.-T. Chuang and L.-Y. Hsu, "Quantum dynamics of molecular ensembles coupled with quantum light: Counter-rotating interactions as an essential component," Phys. Rev. A **109**, 013717 (2024).
[74]J.-F. Huang, J.-Q. Liao, L. Tian, and L.-M. Kuang, "Manipulating counter-rotating interactions in the quantum Rabi model via modulation of the transition frequency of the two-level system," Phys. Rev. A **96**, 043849 (2017).